

# Properties of the hard pomeron with a running coupling constant and the high-energy scattering

Mikhail Braun<sup>a,b)</sup>, Gian Paolo Vacca<sup>a,b)</sup> and Giovanni Venturi<sup>b)</sup>

<sup>a)</sup>Department of Particles, University of Santiago de Compostela

<sup>b)</sup>Department of Physics, University of Bologna

<sup>b)</sup>Istituto Nazionale di Fisica Nucleare – Sezione di Bologna.

May 1996

**Abstract.** The equation for the hard pomeron with a running coupling introduced on the basis of the bootstrap requirement is solved numerically. Two supercritical pomerons are found with the intercept minus 1 of the leading one of the order 0.35{0.5 and that of the subleading one half as large. The contribution of multipomeron exchanges is found to be essential only at extremely high energies of the order of 100 TeV. Comparison of the cross-sections and structure functions to the present experimental data seem to indicate that the asymptotical regime has not yet been achieved.

US-FT/23-96

---

Visiting Professor IBERDROLA. Permanent address: Dep. High-Energy Physics, University of St. Petersburg, 198904 St.Petersburg, Russia

# 1 Introduction.

In recently published papers [1,2] one of the authors has proposed a method to include the running coupling constant into the dynamics of reggeized gluons based on the so-called "bootstrap condition" [3]. This is a relation between the reggeized gluon trajectory

$$\alpha(q) = \frac{N_c}{2} \alpha_s^2 \int_0^1 \frac{d^2 q_1}{(2-\alpha_1)^2} \alpha_1^2 \alpha_2^2; \quad q = q_1 + q_2 \quad (1)$$

and the gluon pair interaction given by the BFKL kernel [4]

$$K_q(q_1; q_1^0) = \frac{1}{2} T_1 T_2 \alpha_s \left( \frac{\alpha_1^2}{\alpha_1^{0^2}} + \frac{\alpha_2^2}{\alpha_2^{0^2}} \right) \frac{1}{(\alpha_1 - \alpha_1^0)^2} \frac{\alpha^2}{\alpha_1^{0^2} \alpha_2^{0^2}} \quad (2)$$

where  $T$  is the gluon colour vector and  $q_1 + q_2 = q_1^0 + q_2^0 = q$ . For the gluon channel  $T_1 T_2 = N_c = 2$  and integrating the kernel one obtains the bootstrap relation [3]

$$\int_0^1 (d^2 q_1 = (2-\alpha_1)^2) K_q^{\text{gluon}}(q; q_1; q_1^0) = \alpha(q) - \alpha(q_1) - \alpha(q_2) \quad (3)$$

This relation guarantees that in the  $t$  channel with the gluon colour quantum number the two gluon system has the reggeized gluon as its state. As a result the production amplitudes in the one-reggeized-gluon-exchange approximation, which serve as an input in the BFKL theory, satisfy unitarity in the leading order [5]. Thereby the whole scheme becomes self-consistent: otherwise one should add to the input amplitudes corrections following from the unitarity. Thus the bootstrap is a crucial element for the reggeization of the gluon and for the theory of the reggeized gluons as a whole. Therefore the only way to introduce the running coupling constant in a manner compatible with the gluon reggeization is to preserve the bootstrap. This was the motivation of the papers [1,2]

Technically this can be achieved if one notices that (3) remains valid if both in the gluon trajectory and interaction each of the momenta squared is substituted by an arbitrary function of it. Indeed, if one takes for the trajectory

$$\alpha(q) = \frac{N_c}{2} \alpha_s(q) \int_0^1 \frac{d^2 q_1}{(2-\alpha_1)^2} \frac{1}{(\alpha_1 - \alpha_1^0)(\alpha_2 - \alpha_2^0)}; \quad q = q_1 + q_2 \quad (4)$$

and for the interaction kernel

$$K_q(q_1; q_1^0) = T_1 T_2 \alpha_s \left( \frac{\alpha_1}{\alpha_1^0} + \frac{\alpha_2}{\alpha_2^0} \right) \frac{1}{(\alpha_1 - \alpha_1^0)(\alpha_2 - \alpha_2^0)} \frac{\alpha(q)}{(\alpha_1^0)(\alpha_2^0)} \quad (5)$$

then (3) will obviously be satisfied as well. The fixed coupling BFKL theory corresponds to a particular choice

$$\alpha(q) = \alpha_s^2 = (2-\alpha_s) \quad (6)$$

The idea of [1,2] was to change  $\alpha(q)$  so that it correspond to a running rather a fixed coupling. For the running coupling some conclusions about the form of  $\alpha(q)$  can be made considering the vacuum channequation in the limiting case of very large  $q$ . Then putting (4) and (5) into the equation and assuming that  $\alpha(q)$  grows with  $q$ , in the leading approximation one gets an evolution equation

$$\partial \alpha(q^2; x) / \partial \ln 1/x = \frac{N_c}{2} \alpha_s^2 \int_0^1 \frac{d^2 q_1}{(\alpha_1 - \alpha_1^0)} \alpha(q_1^2; x) \quad (7)$$

Comparison with the GLAP evolution equation in the leading order in  $\ln 1/x$  (that is, in the double log approximation) allows to find the asymptotic form of  $\alpha(q)$ :

$$\alpha(q) \sim \alpha_s^2 = (2 - \alpha_s(q^2)); \quad q \rightarrow 1 \quad (8)$$

It evidently differs from the fixed coupling case by changing the fixed coupling constant  $\alpha_s$  to a running one  $\alpha_s(q^2)$ . As a result, with a running coupling, both the gluon trajectory and its interaction have to be changed simultaneously in an interrelated manner, so that the resulting equation is different from the BFKL one already in the leading order.

The behaviour of  $\alpha(q)$  at small  $q$ , comparable or even smaller than the QCD parameter  $\Lambda$ , cannot be established from any theoretical calculation, since this domain is nonperturbative. In [1,2] these confinement effects were parametrized by an effective "gluon mass"  $m$ , choosing  $\alpha(q)$  in the form

$$\alpha(q) = (b-2) (q^2 + m^2) \ln((q^2 + m^2) = \Lambda^2) \quad (9)$$

with  $b = (1/4)(11 - (2/3)N_F)$  and  $m$ , which agrees with (8) for large  $q$  and remains finite up to  $q = 0$ .

A preliminary study of the properties of the pomeron with  $\alpha(q)$  given by (9) was performed by the variational technique in [1,2]. It was found that the intercept depended on the ratio  $m = \Lambda$  quite weakly: as  $m = \Lambda$  changes from 1.5 to 5.0 the intercept ( $\alpha$  minus one) falls from 0.4 to 0.25. On the other hand, the slope depends on this ratio very strongly. This allows to fix the ratio  $m = \Lambda$  to values in the interval 3.0 - 4.0.

This variational study, although very simple, cannot however give values for the intercept and especially for the slope with some precision. Still less can be found by this method about the properties of the pomeron wave function essential for the high-energy behaviour of the physical amplitudes [6]. Finally, one does not receive any knowledge about the existence of other solutions with a positive intercept. All these reasons give us a motivation to undertake a numerical study of the two-gluon vacuum channel equation with the gluon trajectory and interaction given by (4) and (5) respectively and the function  $\alpha(q)$  satisfying (8). Its concrete form has been chosen to be slightly more general than (9):

$$\alpha(q) = (b-2) f(q) \quad (10)$$

where

$$f(q) = (q^2 + m_1^2) \ln((q^2 + m^2) = \Lambda^2) \quad (11)$$

It allows for the freezing of the coupling and the confinement proper to occur at somewhat different scales ( $m$  and  $m_1$  respectively). However, on physical grounds, one feels that they should be of the same order.

In sections 2 and 3 we present the basic equations in the form suitable for numerical analysis for the cases  $q = 0$  (forward scattering) and  $q \neq 0$ . In Section 4 we describe the method of the solution and present the numerical results for the intercept, slope and the wave function at  $q = 0$ . The results for the intercept and slope, on the whole, agree with those found in [1,2] by the variational approach. An interesting new result is the existence of a second pomeron with the intercept, roughly speaking, two times less than for the leading one, but still positive. In Section 5 these results are applied to study

the asymptotical behaviour of the cross-section for the scattering. Our conclusions are presented in Section 6.

## 2 Basic equations. Pomeron at $q = 0$

We consider the physical case  $N_c = 3$ . The units are chosen to have  $\alpha_s = 1$ . In relating to observable quantities we take  $\sqrt{s} = 0.2 \text{ GeV}$ .

The pomeron equation is the eigenvalue equation

$$(\hat{L}(q_1) - \hat{L}(q_2)) \psi(q_1) + \int^Z (d^2 = (2 - \alpha_s)^2) K_q^{\text{vac}}(q_1; q_1^0) \psi(q_1^0) = E(q) \psi(q_1) \quad (12)$$

where the "energy" eigenvalue  $E(q)$  is related to the pomeron trajectory via

$$\alpha(q) = 1 + E(q) = 1 + \alpha_0 q^2 \quad (13)$$

The last equation, valid for small  $q$  defines the intercept and the slope  $\alpha_0$ . In (12) the trajectories  $\hat{L}$  and the kernel  $K^{\text{vac}}$  are given by the Eqs. (4) and (5) with  $T_1 T_2 = 3$  and the function  $\psi$  given by (10) and (11). To symmetrize the kernel we pass to the function

$$\psi(q_1) = \psi(q_1) = \int^P \frac{1}{\psi(q_1) \psi(q_2)} \quad (14)$$

We also take out the common numerical factor  $6 = (11 - 2 = 3N_F)$  and express all terms via the function  $f(q)$  defined by (11). Then the equation for  $\psi$  takes the form

$$A_q \psi(q_1) \psi(q_1) + \int^Z d^2 q_1^0 L_q(q_1; q_1^0) \psi(q_1^0) = E(q) \psi(q_1) \quad (15)$$

Here the "kinetic energy" is

$$A_q \psi(q_1) = (1=2) \int^Z \frac{d^2 q_1^0 f(q_1)}{f(q_1^0) f(q_1 - q_1^0)} + (1=2) \int^Z \frac{d^2 q_2^0 f(q_2)}{f(q_2^0) f(q_2 - q_2^0)} \quad (16)$$

The interaction kernel consists of two parts, a quasilocal and a separable ones:

$$L = L^{(ql)} + L^{(sep)} \quad (17)$$

They are given by

$$L_q^{(ql)}(q_1; q_1^0) = \int^S \frac{f(q_1)}{f(q_2) f(q_1 - q_1^0)} \frac{1}{f(q_1^0)} \int^S \frac{f(q_2^0)}{f(q_1^0)} \int^S \frac{f(q_2)}{f(q_1) f(q_2 - q_2^0)} \int^S \frac{f(q_1^0)}{f(q_2^0)} \quad (18)$$

and

$$L_q^{(sep)}(q_1; q_1^0) = \int^P \frac{f(q)}{f(q_1) f(q_2) f(q_1^0) f(q_2^0)} \quad (19)$$

Both parts are evidently symmetric in  $q_1$  and  $q_1^0$ . The scaled energy is related to the initial one by

$$E = \frac{6}{(11 - (2=3)N_F)} \quad (20)$$

Eq. (15) simplifies in the case when the total momentum of the two gluons is equal to zero. With  $q = 0$  the two parts of the kinetic energies become equal and the square roots in (18) turn to unity. So at  $q = 0$  the equation retains its form (15) with

$$A_0 \psi(q_1) = \int^Z \frac{d^2 q_1^0 f(q_1)}{f(q_1^0) f(q_1 - q_1^0)} \quad (21)$$

and the interaction given by (17) where now

$$L_0^{(q1)}(q_1; q_1^0) = \frac{2}{f(q_1) f(q_1^0)} \quad (22)$$

has really become local and

$$L_0^{(sep)}(q_1; q_1^0) = \frac{f(0)}{f(q_1) f(q_1^0)} \quad (23)$$

This is the equation which we shall solve numerically.

To make it one-dimensional we introduce the angular momentum of the gluons  $n$  and choose the solution in the form

$$(q) = \chi_n(q^2) \exp i n \phi \quad (24)$$

where  $\phi$  is the azimuthal angle. Integrating over it in the equation, we obtain an one-dimensional integralequation for the radial function  $\chi_n(q^2)$ :

$$A_0(q) \chi_n(q^2) + \int_0^Z dq_1^2 L_n(q^2; q_1^2) \chi_n(q_1^2) = \chi_n(q^2) \quad (25)$$

with the kernel now given by

$$L_n(q^2; q_1^2) = B_n(q^2; q_1^2) + \chi_{n0} \frac{f(0)}{f(q) f(q_1)} \quad (26)$$

where

$$B_n(q^2; q_1^2) = \int_0^Z d\phi \frac{\cos n\phi}{f(q^2 + q_1^2 - 2q q_1 \cos \phi)} \quad (27)$$

Note that  $A_0$  can be expressed via  $B_0$ :

$$A_0(q) = \int_0^Z dq_1^2 B_0(q^2; q_1^2) \frac{f(q)}{f(q_1)} \quad (28)$$

Evidently Eq. (25) is very similar to a two-dimensional Shroedinger equation with an attractive interaction provided by the local term and a positive kinetic energy described by  $A$ , which however grows very slowly at high momenta (as  $\ln \ln q$  according to [1]). Evidently the attraction becomes smaller with growing  $n$ . So we expect to find negative energies, corresponding to intercepts larger than unity, only for small  $n$ . Remember that for the BFKL pomeron only the isotropic state with  $n = 0$  has a negative energy. Our calculations reveal that the introduction of the running coupling does not change this situation: states with  $|n| > 0$  all have positive energies. So in the following we consider the case  $n = 0$ .

### 3 Pomeron at $q \neq 0$ : the slope

With  $q \neq 0$  the pomeron equation becomes essentially two dimensional. Rather than to attempt to solve it numerically at all  $q$  we limit ourselves to small values of  $q$  and determine not the whole trajectory  $\chi(q)$  but only the intercept  $\chi^0$  defined by (13). This can be done in a much simpler manner using a perturbative approach. We present "the Hamiltonian" in (15)

$$H_q = A_q + L_q \quad (29)$$

in the form

$$H_q = H_0 + W(q) \quad (30)$$

and calculate analytically  $W(q)$  up to terms of the second order in  $q$ . Then for small  $q$  the value of the energy  $\epsilon(q)$  will be given by the standard perturbation formula

$$\epsilon(q) = \epsilon(0) + \langle W(q) \rangle \quad (31)$$

where  $\langle \rangle$  means taking the average with the wave function at  $q=0$ , determined from the numerical solution of the equation discussed in the previous section. Thus we evade solving the two-dimensional problem, but, of course, cannot determine more than the slope. Fortunately it is practically all we need to study the high-energy asymptotics (although, of course, the knowledge of the trajectory as a whole might be of some interest).

In order to derive an expression for  $W(q)$  we pass to the relative momenta  $l$  and  $l^0$

$$q_1 = (l=2)q + l; \quad q_2 = (l=2)q - l; \quad q_1^0 = (l=2)q + l^0; \quad q_2^0 = (l=2)q - l^0 \quad (32)$$

Up to the second order in  $q$  we have

$$f(q_1) = f(l) [1 + a_1(q-l) + \frac{a_1}{4}q^2 + \frac{a_2}{2}(q-l)^2] \quad (33)$$

where

$$a_1 = a_1(l) = 1 + \ln(l^2 + m^2) - \frac{m^2}{l^2 + m^2} - \frac{m_1^2}{f(l)} \quad (34)$$

$$a_2 = a_2(l) = \frac{1}{l^2 + m^2} + \frac{m^2}{(l^2 + m^2)^2} - \frac{m_1^2}{f(l)} \quad (35)$$

The expansion for  $f(q_2)$  differs by changing the sign of  $l$  (or of  $q$ ); for  $f(q_1^0)$  and  $f(q_2^0)$  it suffices to replace  $l$  by  $l^0$  in the expressions for  $f(q_1)$  and  $f(q_2)$ . We use also the notation  $a_1^0 = a_1(l^0)$  and  $a_2^0 = a_2(l^0)$ . We also need the expansion for  $f(q)$ :

$$f(q) = f(0) (1 + a_3 q^2) + O(q^4) \quad (36)$$

where

$$a_3 = \frac{m_1^2}{m^2} + \ln m^2 - \frac{1}{f(0)} \quad (37)$$

The perturbation  $W(q)$ , up to second order in  $q$ , can be expressed via the introduced functions  $a_{1,2}$  and  $a_{1,2}^0$  and the constant  $a_3$ . After some calculations we find a part of  $W$  coming from the kinetic term in Hamiltonian in the form

$$W_1(l) = \frac{1}{2} \int d^2 l^0 \frac{f(l)^n}{f(l^0)} \left[ \frac{1}{f(l-l^0)} + \frac{1}{f(l+l^0)} \right] \left[ a_1^0(q-l^0) \frac{a_1^0}{4} q^2 + a_1^{02} \frac{a_2^0}{2} (q-l^0)^2 + \right. \\ \left. + \frac{a_1 a_1^0 (q-l)(q-l^0)}{f(l-l^0)} + \frac{a_1 a_1^0 (q-l)(q-l^0)}{f(l+l^0)} \right] + A_0(l) \frac{a_1}{4} q^2 + \frac{a_2}{2} (q-l)^2 \quad (38)$$

The part of  $W$  coming from the quasibocal part of the interaction can be written as

$$W_2(l; l^0) = \frac{1}{2} a_1 (q-l) \frac{1}{2} (q-l^0)^2 L_0^{(q1)}(l; l^0) \quad (39)$$

and the one coming from the separable part as

$$W_3(l; l^0) = a_3 \frac{a_1 + a_1^0}{4} q^2 - \frac{1}{2} (a_2 - a_1^2) (q-l)^2 - \frac{1}{2} (a_2^0 - a_1^{02}) (q-l^0)^2 L_0^{(sep)}(l; l^0) \quad (40)$$

As mentioned, only isotropic solutions have the intercept larger than one and are of interest. Then the expression for  $W(q) = \sum_{i=1;2;3}^P W_i$  has to be integrated over the azimuthal angles. Thus integrated values will be denoted  $\hat{W}_i, i = 1;2;3$ . Using (26)–(28), they can be conveniently expressed via the kernel  $B_n$  (eq. (27)):

$$\frac{\hat{W}_1}{2q^2} = \frac{1}{4} \int_0^{\pi/2} d\theta^2 \frac{f(\theta)}{f(\theta^0)} \left[ \frac{a_1^0}{2} + a_1^{\theta^2} \frac{a_2^0}{2} \theta^2 B_0(\theta; \theta^0) - a_1 a_1^0 \theta \theta^0 B_1(\theta; \theta^0) \right] + \frac{A_0(\theta)}{4} a_1 + a_2 \theta^2 \quad (41)$$

$$\frac{\hat{W}_2}{2q^2} = \frac{1}{2} a_1^2 \theta^2 + a_1^{\theta^2} \theta^2 B_0(\theta; \theta^0) + a_1 a_1^0 \theta \theta^0 B_1(\theta; \theta^0) \quad (42)$$

$$\frac{\hat{W}_3}{2q^2} = \frac{f(\theta)}{f(\theta) f(\theta^0)} \frac{h}{2} a_3 - \frac{a_1 + a_1^0}{4} - \frac{1}{4} \theta^2 a_2 - a_1^2 - \frac{1}{4} \theta^2 a_2^0 - a_1^{\theta^2} \quad (43)$$

The slope is given by the momentum average of the sum of these expressions, taken with a given isotropic wave function:

$$s_0 = \frac{\int_0^{\pi/2} d\theta^2 \int_0^{\pi/2} d\theta^0 \frac{f(\theta) f(\theta^0)}{2q^2} \frac{\hat{W}_2 + \hat{W}_3}{\int_0^{\pi/2} d\theta^2 \int_0^{\pi/2} d\theta^0 f(\theta) f(\theta^0)} + \frac{\int_0^{\pi/2} d\theta^2 \int_0^{\pi/2} d\theta^0 f(\theta) f(\theta^0) \hat{W}_1}{\int_0^{\pi/2} d\theta^2 \int_0^{\pi/2} d\theta^0 f(\theta) f(\theta^0)} \quad (44)$$

## 4 Numerical procedure and results

Eq. (25) was first changed to the variable  $t = \ln q^2$  whereupon the wave function and the kernel transform according to

$$(q^2) \rightarrow \tilde{W}(t) = q (q^2) \quad (45)$$

and

$$L(q^2; q_1^2) \rightarrow \tilde{L}(t; t_1) = q q_1 L(q^2; q_1^2) \quad (46)$$

Then the equation was reduced to a finite system of linear equations by approximating the integral by a sum

$$\sum_{i=1}^N \int_{t_i}^{t_{i+1}} dt F(t) \approx \sum_{i=1}^N w_i F(t_i) \quad (47)$$

with points  $t_i$  and weights  $w_i$  depending on the chosen approximation scheme. The final equation is thus

$$\sum_{j=1}^N B_{ij} x_j = x_i; \quad i = 1; \dots; n \quad (48)$$

where

$$x_i = \sum_{j=1}^n \tilde{W}_j \tilde{L}(t_i; t_j) \quad (49)$$

and

$$B_{ij} = A(t_i) \delta_{ij} + \sum_{k=1}^n \tilde{W}_k \tilde{L}(t_i; t_k) \quad (50)$$

A somewhat delicate part of procedure proved to be the integration over the angle in (26), since at large values of  $q^2$  and  $q_1^2$  the integrand becomes strongly peaked at  $\theta = 0$ , so that one should take much care to obtain a reasonable precision.

After determining the lowest eigenvalues and the corresponding eigenvectors  $x_i$  the wave function in the momentum space is directly given by (45) and (49) at points  $q^2 = \exp t_i$ . It should be normalized according to

$$\sum_j \frac{d^2 q}{(2\pi)^2} j(q) f_j = 1 \quad (51)$$

Note that this wave function is a partially amputated one (see Eq. (14)). The full (nonamputated) wave function is given by  $\psi(q) = \psi(q) = \psi(q)$ . It is this function that appears in the physical amplitudes.

The results for the lowest (and negative) eigenvalues of energy for the case  $n = 0$  (isotropic pomeron) are presented in Figs. 1 and 2. Actually energies with an opposite sign are shown, which according to (13) give precisely the intercepts (minus one). As mentioned, the QCD scale here and in the following is taken to be  $\Lambda = 0.2 \text{ GeV}$ . In Fig. 1 the intercepts are shown for the case when the two scales  $m$  and  $m_1$  in (11) are equal. Fig. 2 illustrates the dependence of the intercepts on the ratio  $m = m_1$ . The most interesting observation which follows from these figures at once is that in all cases one observes two positive intercepts, which correspond to two different supercritical pomerons, the leading and subleading ones. The intercept of the leading pomeron is found to be in accordance with our earlier calculations, performed by the variational method (it is slightly larger, which was to be expected). For physically realistic values of  $m$  and  $m_1$  in the interval  $0.5 - 1.0 \text{ GeV}$  it takes on values in the region of  $0.5 - 0.3$  falling with the masses  $m$  and  $m_1$ . The same trend is seen for the intercepts of the subleading pomeron, which lie in the interval  $0.25 - 0.15$ .

The slopes of the two found pomerons are shown in Fig. 3 as a function of  $m$  for the case  $m = m_1$ . The slopes depend very strongly on the value of the regulator mass. The physically reasonable slopes for the dominant pomeron of the order of  $\alpha_0 = 0.25 (\text{GeV} = c)^{-2}$  restrict the values of  $m$  to the region  $0.7 - 0.9 \text{ GeV}$ . So finally we choose

$$m = 0.82 \text{ GeV} \quad (52)$$

which leads to the following parameters of the leading (0) and subleading (1) pomerons

$$\alpha_0 = 0.384; \quad \alpha_0 = 0.250 (\text{GeV} = c)^{-2}; \quad \alpha_1 = 0.192; \quad \alpha_1 = 0.124 (\text{GeV} = c)^{-2} \quad (53)$$

In Fig. 4 we show the coordinate space wave functions  $\psi(r)$  of these two pomerons.

## 5 Pomeron and the high-energy scattering. Discussion

To apply the found results to the actual physical processes one has to couple the pomerons to the external sources corresponding to the colliding particles. The only way to do it in a more or less rigorous manner is to assume that both the projectile and target are highly virtual photons with momenta  $q$  and  $p$  respectively,  $q^2 = Q^2 \gg \Lambda^2$  and  $p^2 = P^2 \gg \Lambda^2$ . Then the nonperturbative effects inside the target and projectile can safely be neglected. As shown in [6] the scattering amplitude in the high colour number limit then takes an eikonal form for fixed transverse dimensions of the projectile and target and leads to a cross-section

$$\sigma = 2 \int d^2R d^2r d^2r^0 \psi_q(r) \psi_p(r^0) (1 - \exp(-z(\alpha; R; r; r^0))) \quad (54)$$

where

$$z(\alpha; R; r; r^0) = (1/8) \int_{-Z}^Z \frac{d^2q d^2q_1 d^2q_1^0}{(2)^6} G(\alpha; q; q_1; q_1^0) \exp i q R \prod_{i=1,2}^Y (1 - \exp i q_i r) (1 - \exp i q_i^0 r^0) \quad (55)$$

is essentially the Fourier transform of the (nonamputated) Green function of Eq. (12),  $G(\alpha; q; q_1; q_1^0)$ , considered as a function of the energetic variable  $\alpha = pq$  and with  $q = q_1 + q_2 = q_1^0 + q_2^0$ . The functions

$\rho_q$  and  $\rho_p$  correspond to the colour densities of the projectile and target photons, respectively. Their explicit form was found in [7] for both transverse and longitudinal photons.

The found supercritical pomeron represent a part of the total pomeron spectrum which contributes to the Green function a term dominating at high energies

$$G_P(l; q; q_1; q_1^0) = \sum_{i=0,1} \gamma_i(q) \gamma_{i-1}(q_1; q_2) \gamma_i(q_1^0; q_2^0) \quad (56)$$

where  $\gamma_i$  and  $\gamma_{i-1}$  are the trajectories and wave functions of the leading (0) and subleading (1) pomerons. At high  $l$  we can neglect the dependence on the total momentum  $q$  of the wave functions, taking them at  $q = 0$ , and approximate the trajectories according to (13). Then all the quantities in (54) become determined, so that we can calculate the cross-sections for both the transversal and longitudinal projectile photon and thus find the structure function of the virtual photon target. We have taken for the latter a transversal photon with the lowest momentum admisible of  $P = 1 \text{ GeV} = c$ . The resulting structure functions are presented in Fig. 5 for the interval of small  $x$  which we extended to extraordinary small values to clearly see the unitarization effects.

To move closer to reality one has to consider hadronic target and projectiles. The confinement effects make any rigorous treatment of such a case impossible. Rather than to introduce arbitrary parameters (in fact, functions) we extend the formula (54) to hadronic target and projectile substituting the photonic colour densities by hadronic ones. For the latter we take a Gaussian form and a normalization which follows from the comparison to the electromagnetic densities with only the simplest quark diagrams taken into account. In particular for the proton we take the Gaussian, with the observed electromagnetic proton radius and normalized to three. Such a treatment, in all probability, somewhat underestimates the density, since it does not include coupling to gluons.

The proton structure functions and the proton-proton total cross-sections which follow from this approximation for the densities are shown in Figs. 6 and 7 respectively. To see the unitarization effects we had again to consider extraordinary high values of  $l=x$  and energies, well beyond our present experimental possibilities.

In discussing these results, we have first to note that their overall normalization is somewhat undetermined, since the exact scale at which enters into  $\ln$  factors is unknown. A second point to note is that the subleading pomeron contribution is always very small: it amounts to a few percent at smallest values of  $l=x$  and  $s$  considered and naturally gets still smaller at higher  $l=x$  or  $s$ .

As one observes from Figs. 5-7, the structure functions and cross-sections monotonously rise with  $l=x$ ,  $s$  and  $Q^2$ . Studying the asymptotics of the solutions of Eq. (12) at high  $q$  and of Eq. (54) one can show that this rise is logarithmic. In particular, the structure function of the virtual photon rises as  $\ln^4(l=x)$  and as  $\ln(q^2)$  with coefficient 2.5. The proton-proton cross-section eventually rise as  $\ln^2 s$ , as expected. Comparison to the Froissart bound (dash-dotted line in Fig. 7) shows however that it remains far from being saturated.

The most interesting result that follows from Figs. 5-7 is that the unitarization effects become visible only at exceedingly very small values of  $x$  or very large values of  $s$ , well outside the range of the present experiment. They appear earlier at lower  $Q^2$ . Still at the smallest value  $Q = 2 \text{ GeV} = c$  considered, the exchange of more than one pomeron achieves only 15% of the total for the proton

structure function at  $x = 10^{-10}$ . Likewise the relative contribution of many pomerons to the proton-proton cross-section rises to 23% only at  $s = 10^5 \text{ GeV}$ .

Comparing the calculated proton structure functions and the cross-sections with the experimental results at highest  $1/x$  and  $s$  available we observe that our results are essentially smaller than the observed ones. Experimental value of  $F_{2p}(Q^2; x)$  at  $Q^2 = 8.5 (\text{GeV}/c)^2$  and  $x = 0.000178$  is  $1.19 \pm 0.05 \pm 0.16 [8]$ . Our calculations only give a value 0.17. The pp cross-section at  $\sqrt{s} = 1800 \text{ GeV}$  is around  $80 \text{ mb}$  [9], whereas our result is  $18.5 \text{ mb}$ . Of course, having in mind the uncertainties in the overall normalization and a very crude picture for the pomeron coupling to the proton assumed, one cannot ascribe too much importance to this fact. However one is tempted to explain this underestimation of the experimental values by the simple reason that we are too far from the pure asymptotical regime yet and that other solutions of Eq. (13) different from the found supercritical pomerons and having their intercepts around unity give the bulk of the contribution at present energies. This may also explain the notorious discrepancy between a high value of the hard pomeron intercept, of the order  $0.35 \pm 0.5$ , and the observed slow growth of the experimental cross-section, well described by the "soft pomeron" with an intercept around 0.08.

If this picture is correct then we may expect that with the growth of energy the cross-sections will grow faster and faster, until at  $\sqrt{s} = 10 \text{ TeV}$  they will become well described by a pure hard pomeron with the intercept  $0.35 \pm 0.5$ . This power growth will continue until energies of an order  $1000 \text{ TeV}$  when finally the unitarity corrections set in to moderate the growth in accordance with the Froissart bound.

## 6 Conclusions

The result of our study show that with the running coupling included the pomeron equation possesses bound state solutions which have negative energy and thus intercepts greater than unity. These solutions correspond to supercritical pomerons in the old sense, that is, they represent simple poles in the complex angular momentum plane. A new result is that two such pomerons appear. However the subdominant pomeron does not seem to play any role in describing the asymptotical behaviour of the amplitudes. The intercepts of the pomerons depend weakly on the infrared regulator parameter and stay in the region  $0.35 \pm 0.5$  for its physically reasonable values. The introduction of the running coupling and thus a scale provides for a nontrivial slope for the pomeron, which is responsible for the physically reasonable behaviour of the cross-sections at very high energies.

For realistic photonic cross-sections and with a rather crude approximation for the hadronic ones unitarization effects begin to be felt at extraordinary high energies, of the order  $100 - 1000 \text{ TeV}$  (or equivalently  $x < 10^{-10} - 10^{-12}$ ). Until these energies a single pomeron exchange remains a very good approximation to the asymptotic amplitude.

Comparison to the experimental cross-sections and structure functions at the highest energy (lowest  $x$ ) achieved seems to confirm the widespread opinion that we are still rather far from the asymptotical regime and that other states, different from the supercritical pomerons, give the dominant contribution.

## 7 Acknowledgments.

The authors express their gratitude to Prof. C Pajares for his attention and helpful discussions. M A B thanks the INFN for financial help during his stay at Bologna University and IBERDROLA for financial support during his stay at the University of Santiago de Compostela. G P Vacca thanks Profs. C Pajares and L Miramontes for their hospitality during his stay at the University of Santiago de Compostela.

## 8 References.

1. M A Braun, Phys. Lett. B 345 (1995) 155.
2. M A Braun, Phys. Lett. B 348 (1995) 190.
3. L N Lipatov, Yad. Fiz. 23 (1976) 642.
4. V S Fadin, E A Kuraev and L N Lipatov, Phys. Lett. B 60 (1975) 50.
- I.I. Balitsky and L N Lipatov, Sov J Nucl Phys. 15 (1978) 438.
5. J Bartels, Nucl. Phys. B 151 (1979) 293.
6. M A Braun, Phys. Lett. B 357 (1995) 138
7. N N Nikolaev and B G Zakharov, Z Phys. C 49 (1991) 607
8. H1 Collab., Nucl. Phys. B 439 (1995) 471
9. See M Block et al in Proc. 24th Int. Symp. on Multiparticle Dynamics, Ed. A Giovannini, World Scie. (1995).

## 9 Figure captions

Fig. 1 Pomeron intercepts as a function of the infrared regulator mass  $m = m_1$ ;  $\gamma = 0.2 \text{ GeV}$ .

Fig. 2. Pomeron intercepts for different values of the confinement parameter  $m_1$  and the coupling freezing parameter  $\gamma$ .

Fig. 3. Pomeron slopes as a function of the infrared regulator mass  $m = m_1$ ;  $\gamma = 0.2 \text{ GeV}$ .

Fig. 4. Coordinate space wave functions for the leading ( $\phi_0(r)$ ) and subleading ( $\phi_1(r)$ ) pomerons. Both  $r$  and  $b$  are in units  $1/b = 1 \text{ fm}$

Fig. 5. Structure functions of a virtual photon ( $Q^2 = 1 \text{ GeV}^2$ ) at  $Q^2 = 4$  and  $100 \text{ (GeV}^2)$  as a function of  $x$  (solid curves). Dashed curves show the contribution of a single pomeron exchange.

Fig. 6. Proton structure functions at  $Q^2 = 4$  and  $100 \text{ (GeV}^2)$  as a function of  $x$  (solid curves). Dashed curves show the contribution of a single pomeron exchange.

Fig. 7. Proton-proton total cross-sections as a function of cm. energy  $\sqrt{s}$  (the solid curve). The dashed curve shows the contribution of a single pomeron exchange. The dash-dotted curve marks the Froissart bound.

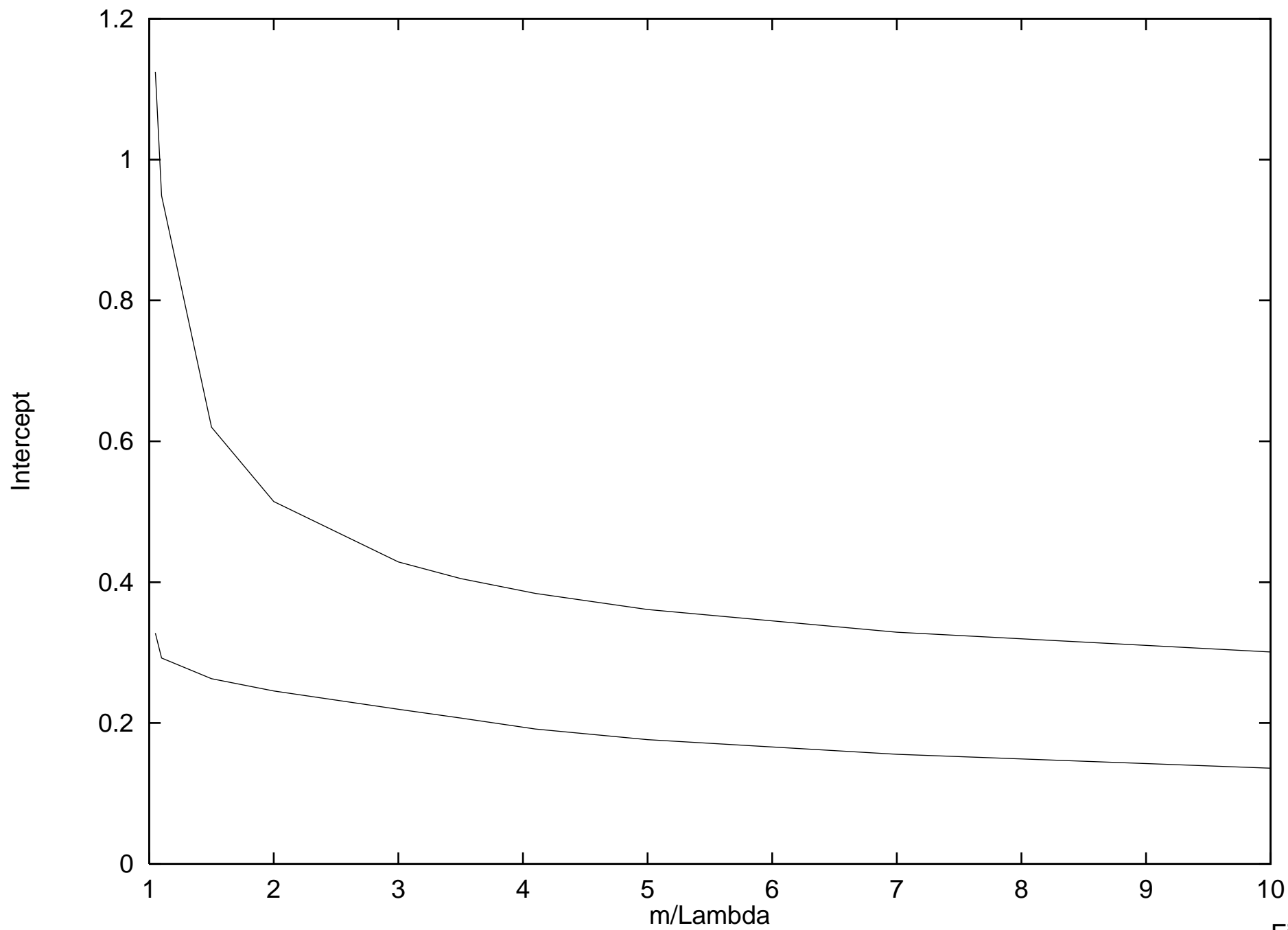


Fig. 1

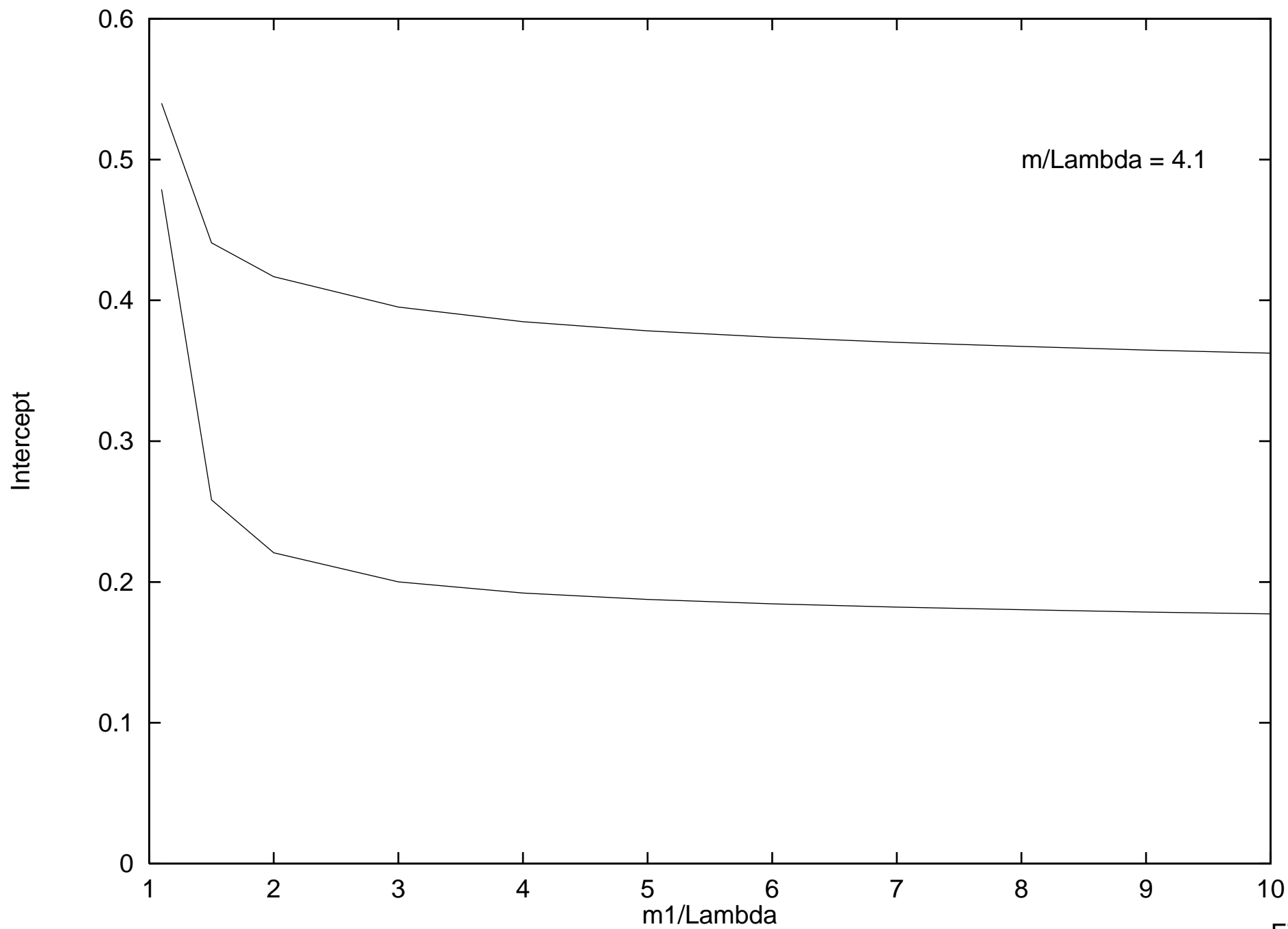


Fig. 2

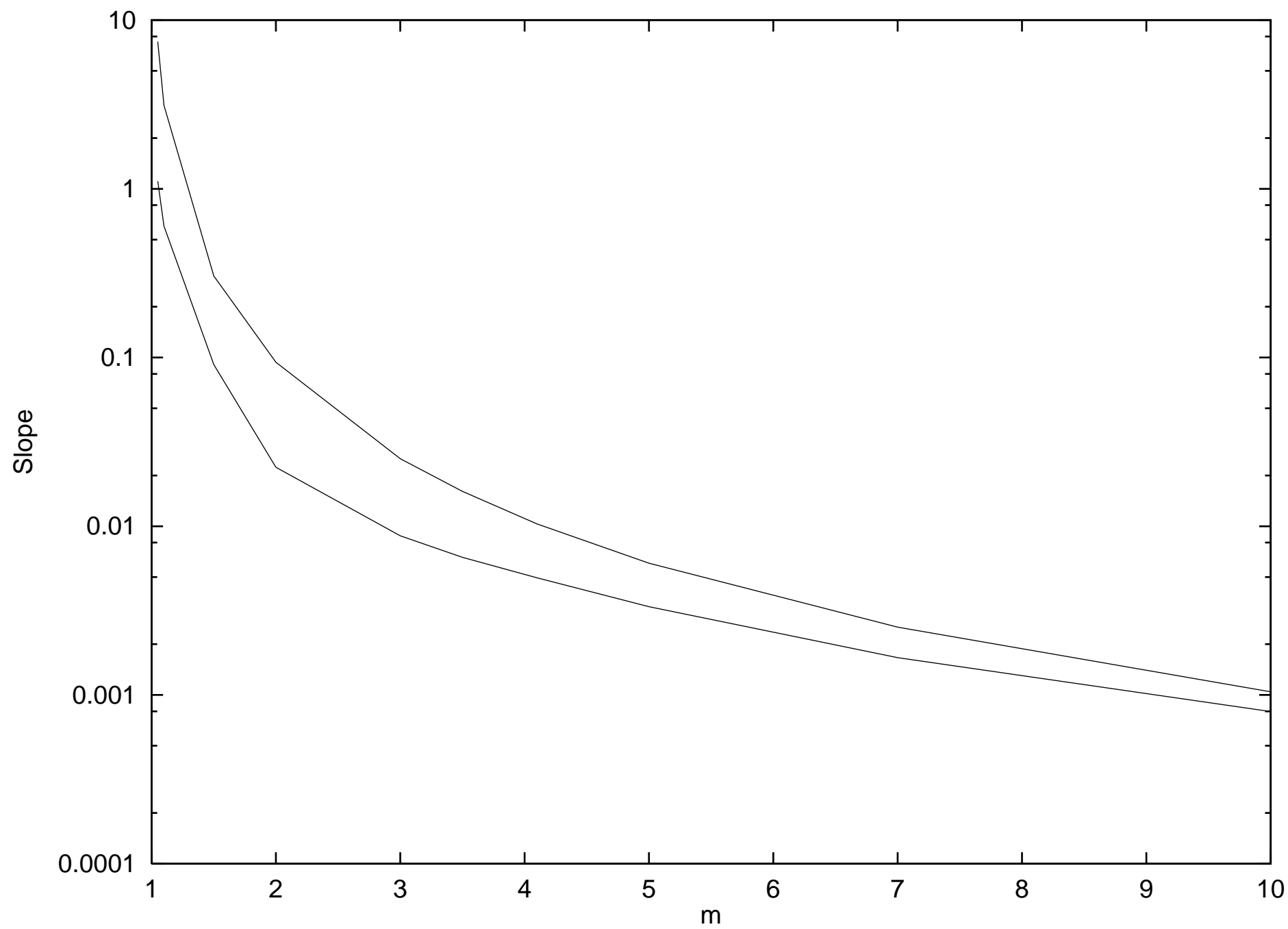


Fig. 3

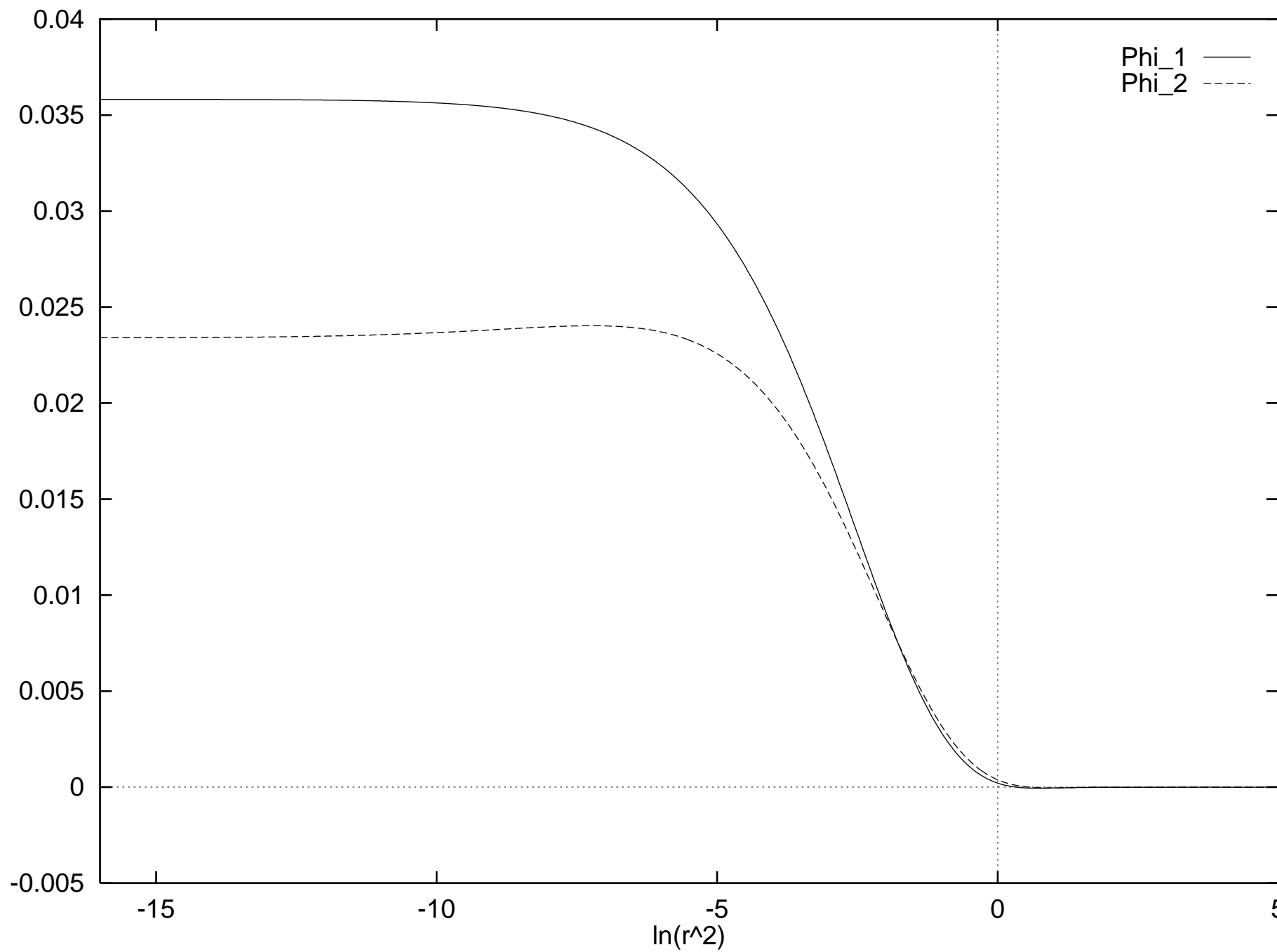


Fig. 4

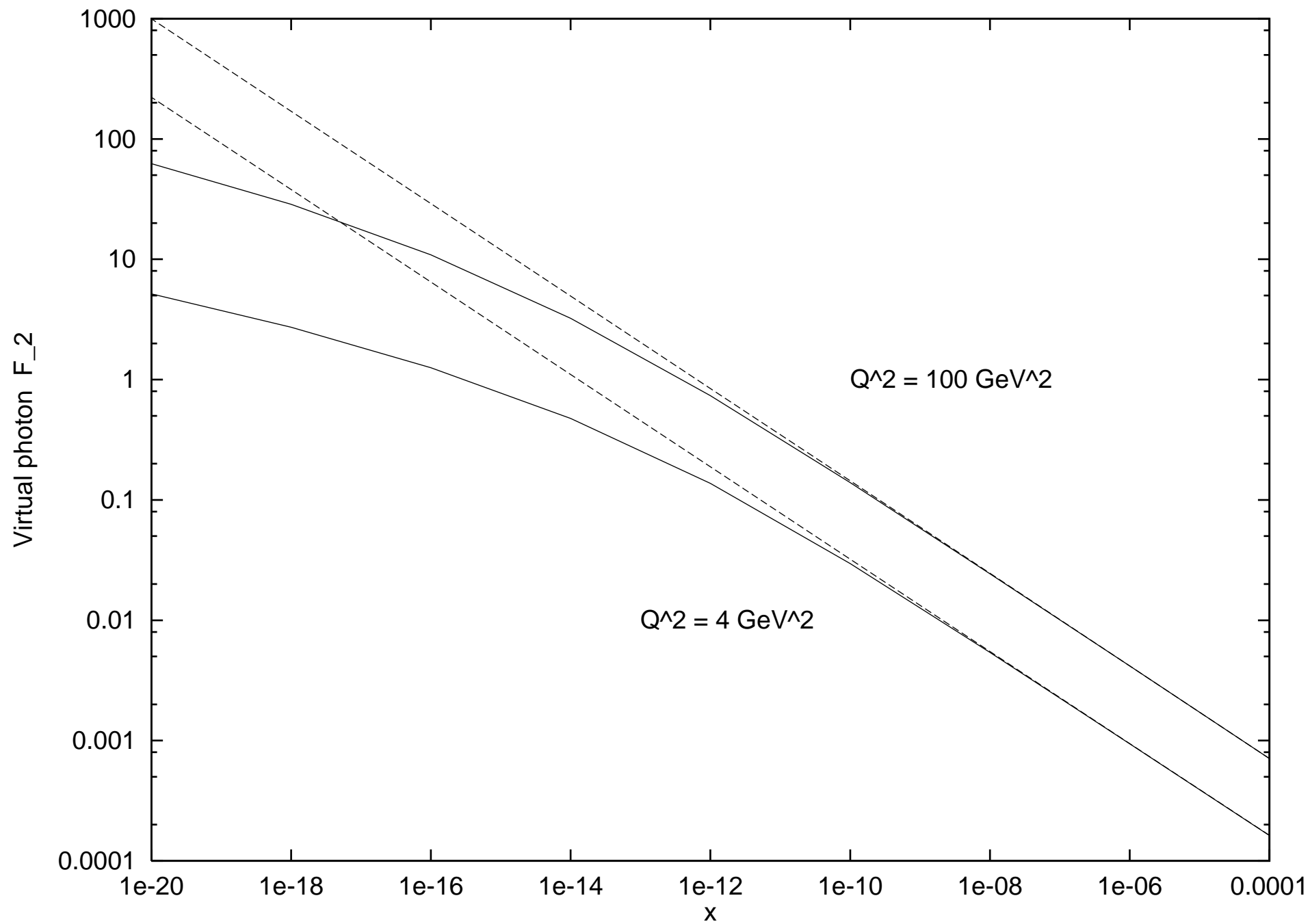


Fig. 5

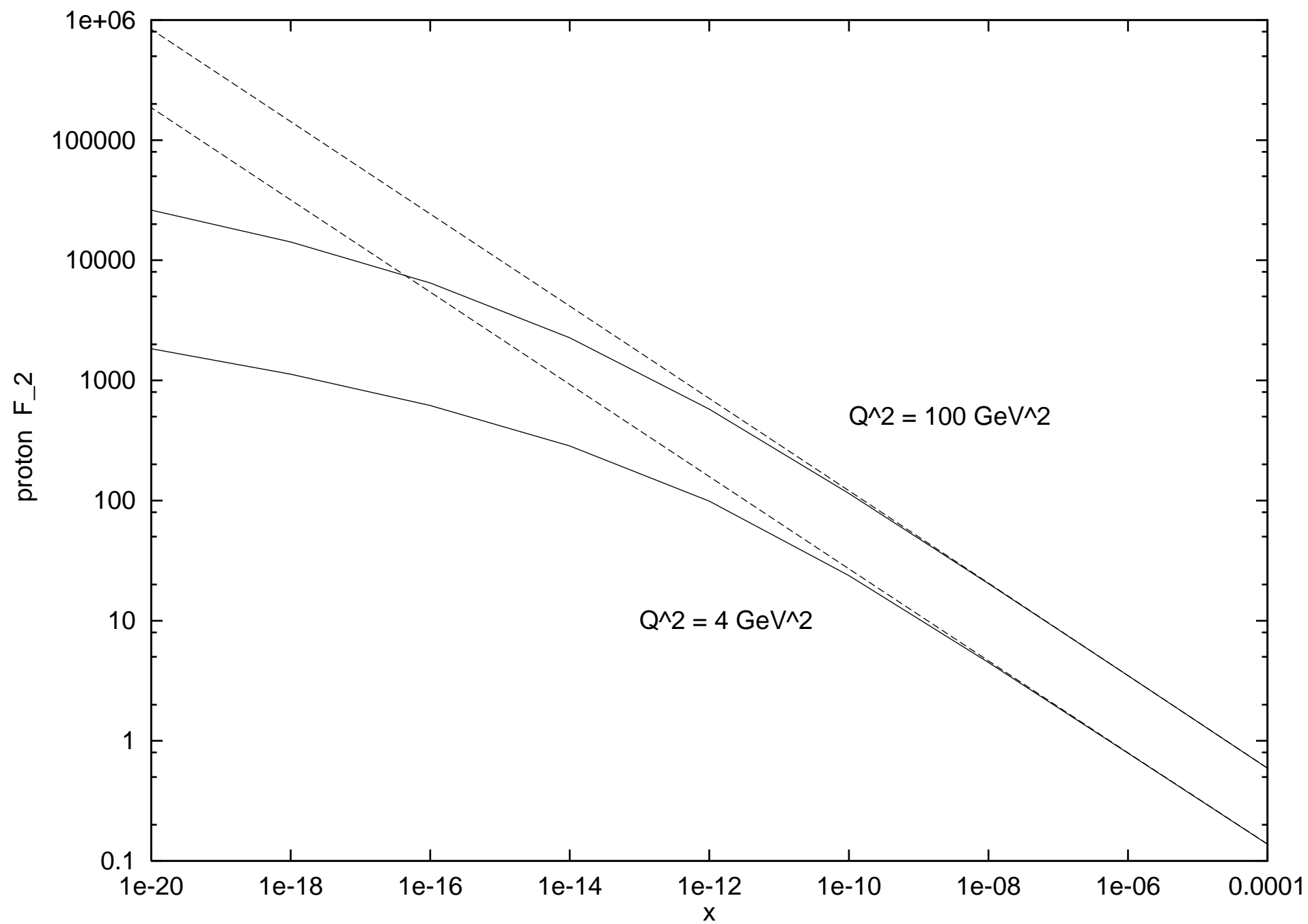


Fig. 6

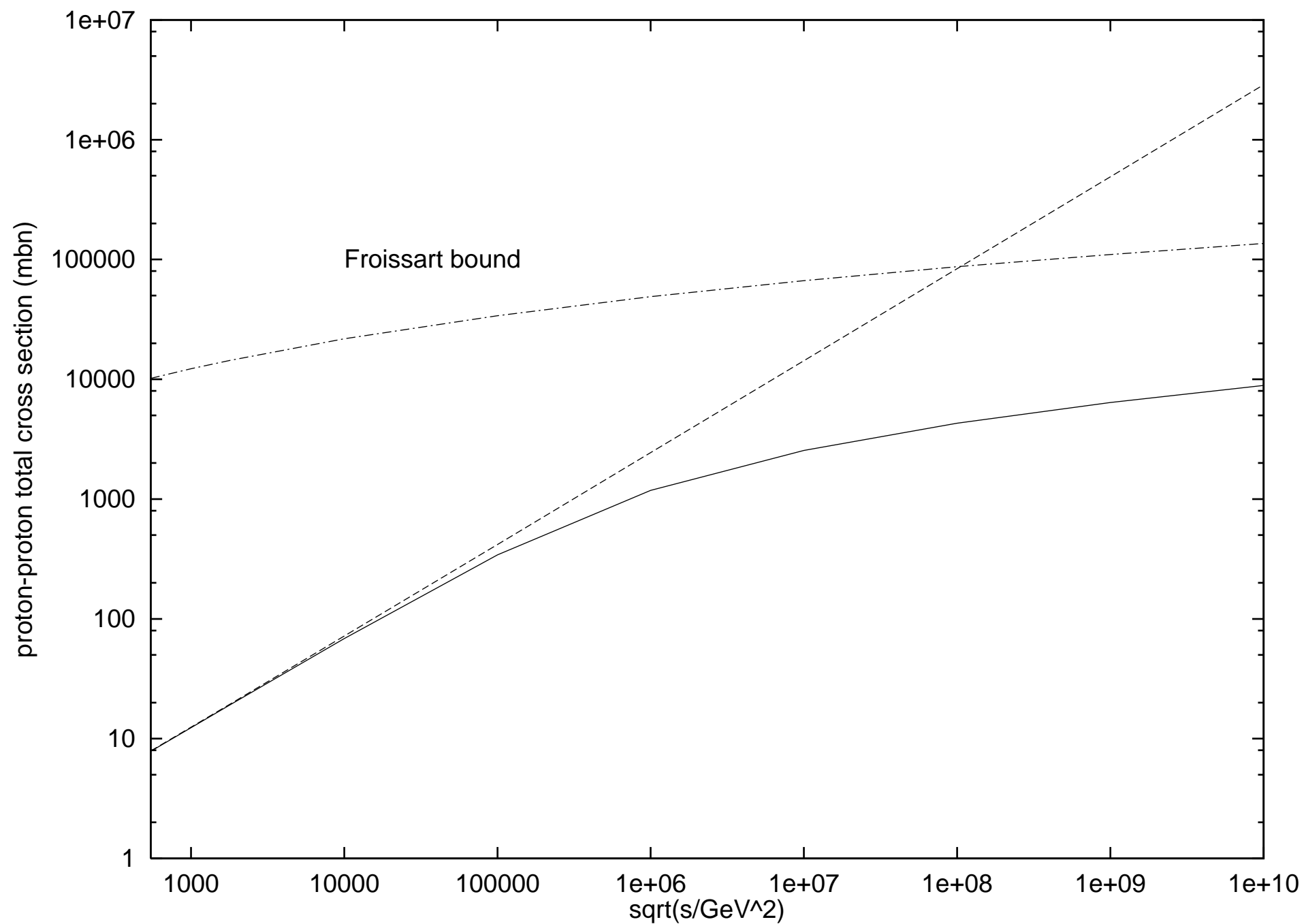


Fig. 7